THE JOURNAL OF
PHYSICAL CHEMISTRY A

Glass-Forming Properties of 3-Methylbutane-1,2,3-tricarboxylic Acid and Its Mixtures with Water and Pinonic Acid

Hans P. Dette,[†,‡] Mian Qi,[†,‡] David C. Schröder,[†] Adelheid Godt,[†,‡] and Thomas Koop*[†,‡]

[†]Faculty of Chemistry and [‡]Center for Molecular Materials, Bielefeld University, Universitätsstraße 25, D-33615 Bielefeld, Germany

Supporting Information

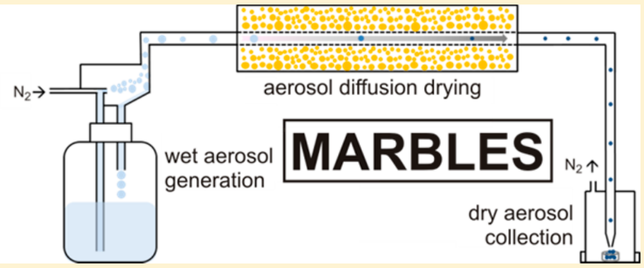

ABSTRACT: 3-Methylbutane-1,2,3-tricarboxylic acid (3-MBTCA) is an atmospheric oxidation product of α-pinene and has been identified as the most relevant tracer compound for atmospheric terpene secondary organic aerosol (SOA) particles. Little is known, however, of its physicochemical properties such as water solubility and phase state (e.g., liquid, crystalline, glassy). To gain knowledge, we synthesized 3-MBCTA from methyl 2-methylpropanoate and dimethyl maleate via a Michael addition and subsequent hydrolysis with 78% overall yield. It was found that 3-MBTCA transforms into anhydrides upon melting at $T_m = 426 \pm 1$ K, thus preventing a determination of the glass transition temperature T_g by differential scanning calorimetry (DSC) through melting and subsequent cooling. Therefore, we designed the novel technique MARBLES (metastable aerosol by low temperature evaporation of solvent) for transferring a substance into a glassy state without heating. In MARBLES an aqueous solution is atomized into wet aerosol particles that are subsequently dried in several diffusion dryers resulting in glass formation of the residual particles for several solutes. The glassy aerosol particles are collected in an impactor until enough mass has accumulated that the sample's T_g can be determined by DSC. Using this method, the glass transition temperature of 3-MBTCA was found to be $T_g \approx 305 \pm 2$ K. Moreover, we have determined the glass transition T_g' of the maximal freeze-concentrated aqueous solution of 3-MBTCA, and T_g of mixtures of 3-MBTCA with water and pinonic acid. The latter data indicate a dependence of T_g upon the atomic oxygen-to-carbon ratio of the mixture, with implications for parametrizing the glass-forming behavior of α-pinene SOA particles in the atmosphere.

1. INTRODUCTION

Aerosols influence various processes in Earth's atmosphere. For example, they directly affect Earth's albedo through scattering and absorption of incoming sunlight, which in turn depend upon the aerosol particles' properties such as phase state, size, chemical composition, and absorption cross section.[1] Aerosols further influence the atmosphere's radiative transfer indirectly by serving as cloud condensation nuclei (CCN) or ice nuclei (IN), partly depending on the pre-existing aerosol particles' phase state.[2−4] For example, liquid particles of water-soluble compounds may act as CCN for liquid water clouds and solid particles, both crystalline and amorphous ones, may act as IN for ice clouds[5−8] The magnitude of their influence is little understood,[9] in part because aerosol properties such as phase state are often variable and not well-known. This is particularly true for organic aerosols that make up for about half of the aerosol mass in the atmosphere.[10−13]

Most organic molecules are released into the atmosphere as volatile organic compounds from which secondary organic aerosol (SOA) particles may arise through atmospheric oxidation and subsequent condensation.[10,13−15] The organic compounds found in organic aerosols often show moderate to good water solubility due to their high oxidation state. For example, atmospheric organic aerosols may consist of compounds such as mono-, di-, or tricaboxylic acids, polyols, ketones, aldehydes, different mono- and disaccharides, and others.[10,16−18] In contrast to most inorganic aerosol particles, which crystallize readily upon drying,[19] the organic aerosol particles rather tend to form liquid particles instead of crystals due to being a mixture of compounds.[20]

SOA particles arising from the oxidation of biogenic precursors and subsequent condensation consist of hundreds of different organic compounds, but a number of key components have been identified. For example, in boreal forests α-pinene is one of the most important biogenic SOA precursors.[10,14,21] Experiments have shown that the gas-phase oxidation of α-pinene proceeds via pinonic acid, a semivolatile compound, to the second-generation oxidation product 3-methylbutane-1,2,3-tricarboxylic acid (3-MBTCA), a low-volatile compound found predominantly in the aerosol phase, Figure 1.[13,14,22−27] Not much is known about the physicochemical properties and the phase state of pinonic acid and 3-MBCTA, neither as pure components nor in mixtures. This knowledge is, however, particularly important, because it has been suggested that SOA particles in boreal forests may exist in an amorphous solid, i.e., glassy state at room temperature under

Received: June 13, 2014
Revised: August 6, 2014
Published: August 6, 2014

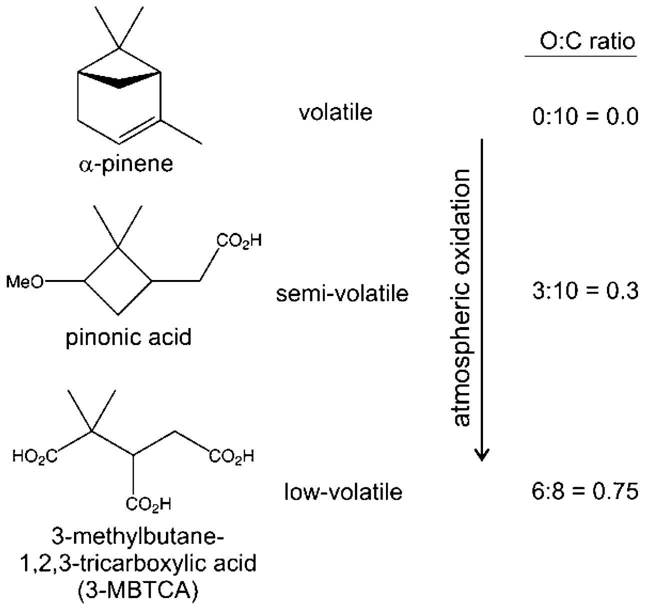

Figure 1. Structures and properties of marker compounds during the atmospheric oxidation of α-pinene.

dry conditions.[28,29] A semisolid or solid state of organic aerosol particles has important atmospheric implications such as delayed gas-to-aerosol partitioning.[27,30−33] Moreover, such particles may also have a longer chemical lifetime as the oxidation can take place only on the surface of glassy particles because of inhibited diffusion in the bulk of a particle.[31,34−38] The glass-forming properties of key compounds of oxygenated organic aerosol such as 3-MBTCA have not been investigated experimentally until now.[29] Because of its atmospheric relevance, we synthesized 3-MBTCA and conducted a physicochemical characterization of 3-MBTCA in the pure state and in mixtures with water and pinonic acid.

For the estimation of whether a SOA compound such as 3-MBTCA may form a glass in the atmosphere, it is essential to determine its glass transition temperature T_g. The most common approach for the determination of T_g is to transfer a sample into a glass by first melting it by heating and subsequently cooling it to temperatures sufficiently below the estimated T_g, which typically is about 0.7 times its melting temperature.[29] Then the sample is reheated at a constant heating rate and the glass transition is detected by means of differential scanning calorimetry (DSC) through the associated change in heat capacity.[39,40] The approach described here works for many substances, but it requires two important preconditions to be fulfilled: first, the substance must remain chemically intact upon melting and, second, the substance must not recrystallize upon cooling but instead remain in a supercooled metastable liquid state until the glass transition is reached. However, in particular, sugars or di- and tricarboxylic acids including 3-MBTCA undergo chemical changes upon melting. Hence alternative methods for glass formation must be chosen, for example, by drying a solution of the substance of interest.[41] The most common approaches are freeze-drying or simple heating. In freeze-drying it is difficult to ensure complete dehydration of a glassy sample, because of the rather small water diffusion coefficient in glassy samples at low temperature[42] and, thus, freeze-drying a sample may require a significant amount of time. Drying by heating may enhance the likelihood of crystallization and bears the risk of chemical changes in heat-unstable samples. These potential risks apply to heat drying of bulk samples as well as to spray drying, in which the sample solution is first sprayed into an aerosol before being heated by mixing with a hot gas.[43,44]

To circumvent these problems, we have developed the MARBLES method (metastable aerosol by low temperature evaporation of solvent), which is described herein. MARBLES is based on diffusion drying of an aerosol at room temperature and has three principal advantages: relatively fast drying on the order of seconds to minutes, a reduced likelihood of nucleation of crystalline phases in the small, typically micrometer- to submicrometer-sized liquid aerosol droplets, and avoidance of chemical changes of organic substances by operating at room temperature. Below, we will show the functionality of the method using different substances with known T_g before we apply it to 3-MBTCA and its mixtures with water and pinonic acid.

The paper is structured as follows: Section 2 presents the synthesis and characterization of 3-MBTCA. Section 3 describes experimental details of the DSC measurements and the new experimental method MARBLES as well as several validation experiments with reference substances. In section 4, the results of glass transition measurements of pure 3-MBTCA and its mixtures with water and pinonic acid are presented as well as a discussion of atmospheric implications, before we finish with a conclusion and a brief outlook in section 5.

2. SYNTHESIS AND CHARACTERIZATION OF 3-MBTCA

To obtain 3-MBTCA, we first pursued the route outlined by Szmigielski,[25] i.e., the deprotonation of dimethyl succinate, substitution reaction between the resulting enolate and methyl 2-bromo-2-methylpropanoate, and finally ester hydrolysis. However, in our hands the substitution reaction gave a very low conversion of about 26% and side products. Therefore, we developed an alternative method (Scheme 1): first deprotonation of methyl 2-methylpropanoate (**1**), second Michael addition of the resulting enolate to dimethyl maleate (**2**)[45] resulting in the trimethyl ester (**3**) of 3-MBTCA, and third

Scheme 1. Synthesis of 3-MBTCA

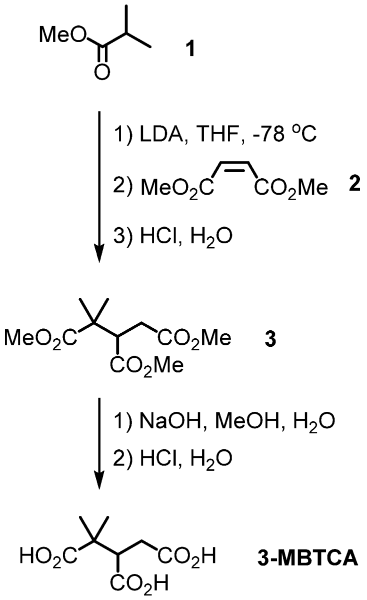

ester hydrolysis yielding the desired 3-MBTCA. This simple three-step synthesis provided pure 3-MBTCA in 78% yield from very cheap starting compounds. Details of the preparation are given in the Supporting Information.

The melting point of 3-MBTCA was determined with DSC measurements (see below) by heating a few crystals (about 5.1 mg) at a heating rate of 10 K min^{-1} to give $T_m = 426 \pm 1$ K, in good agreement with literature data of T_m = 427−428 K.[46] Furthermore, we determined the solubility of 3-MBTCA in water at 293.15 K by drying about 0.3 or 1 g of a saturated solution and weighing the resulting residue, yielding a solubility value of about 320 g of 3-MBTCA per liter of water, corresponding to a solute mass fraction of $w_{sol} \approx 0.24 \pm 0.02$. The water activity and density of an aqueous solution with a mass fraction of $w = 0.2$ were determined to be $a_w = 0.982$ and $\rho = 1.05(8)$ g cm^{-3} using a water activity meter (Decagon model series 3 TE) and a density meter (Anton Paar, DMA 4500 M).

3. THERMAL CHARACTERIZATION TECHNIQUE AND SAMPLE PREPARATION WITH MARBLES

3.1. Differential Scanning Calorimetry. Differential scanning calorimetry (DSC) is a standard technique for studying phase transition processes such as crystallization, melting, and glass formation. For the experiments described below we used a differential scanning heat-flow calorimeter (Q100, TA Instruments) that was calibrated comprehensively using a series of nine calibration standards at cooling and heating rates between −10 and +10 K min^{-1}.[47] The resulting temperature accuracy of the calorimeter is about ±0.2 at 1 and ±0.4 K at 10 K min^{-1}. In a typical measurement, 1−10 mg of a sample was placed in an aluminum pan (thereafter sealed hermetically), which was then transferred into the calorimeter. Measurements were performed with an empty pan as a reference. The glass transition temperature T_g of a sample was determined in the heating mode at 10 K min^{-1} using the onset of the glass transition signal, i.e., the intersection between the extrapolated baseline and a line of maximum slope in the heat flow signal, following the convention of Angell.[39] We note that because of small ambiguities in the evaluation of these slopes and the repeatability of the experimentally determined T_g values across multiple samples, we estimate the accuracy of the glass transition temperatures given below to be about ±2 K.

3.2. The MARBLES Method. We have developed and tested a novel method for preparing glassy samples of water-soluble substances which we term MARBLES for "metastable aerosol by low temperature evaporation of solvent". With the MARBLES method an aqueous solution of a compound is sprayed into an aerosol followed by drying of the aerosol droplets and collection of the dry particles. This is similar to classical spray drying, but MARBLES avoids heating of the sample and requires only a small amount of material for preparing samples that can be analyzed by DSC. MARBLES has several key advantages. First, drying of aqueous bulk samples or droplets with a diameter of several micrometers or more can be time-consuming, because of the small water diffusivity in glassy materials.[42,48] However, under the same conditions drying of submicrometer aerosol particles (see images of collected particles in Figure S3 in the Supporting Information) can be achieved on the time scale of seconds to minutes.[29,34,49,50] This is made use of in MARBLES. Second, the crystallization probability of the solute compound is strongly reduced in aerosol particles, because of the smaller volume and the absence of solid impurities such as dust in most aerosol droplets that might trigger crystal nucleation. And third, the entire procedure (dissolution and drying) can be performed at room temperature, thus eliminating the occurrence of chemical changes which are often found when bulk samples are melted (see below).

Figure 2a outlines the working principle of the MARBLES method. A dilute aqueous solution of the substance of interest is atomized into a wet aerosol by an aerosol generator. The aerosol is dried by diffusion drying before the aerosol particles are collected in an impactor. A detailed functional scheme of the MARBLES setup is shown in Figure 2b. Aerosol particles are produced with an atomizer (A) by nitrogen purge gas from a pressurized nitrogen source (NS), following the general working principle of the constant output atomizer design of Liu and Lee.[51] The aerosol flow is directed through a drying section consisting of three homemade diffusion dryers (DD), each 80 cm long. Each diffusion dryer consists of an outer tube made

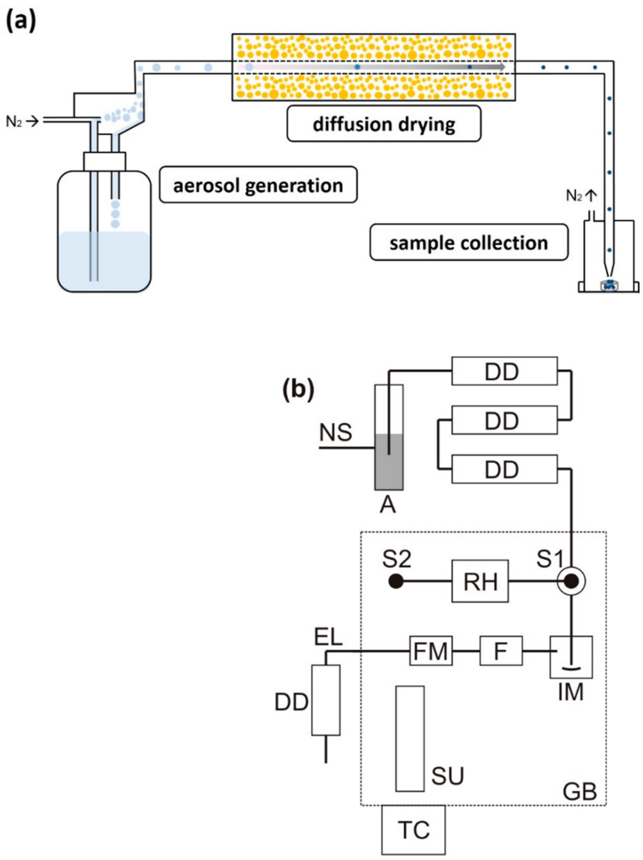

Figure 2. (a) Working principle of the MARBLES system: wet aerosol generation from an aqueous solution in an atomizer, aerosol drying in diffusion dryer, and dry aerosol collection in an impactor. (b) Detailed sketch of the MARBLES system. A nitrogen source (NS) is used to drive an atomizer (A) for aerosol generation, the drying section consists of several diffusion dryers (DD), a hygrometer for relative humidity measurement (RH) with a sensor (S1) in the aerosol flow, and a sensor (S2) in the dry glovebox (GB). Dried particles are collected in an impactor (IM) and residual aerosol particles are filtered out (F). The overall aerosol flow rate is measured with a flow meter (FM). The exhaust line (EL) is protected from room air humidity by another diffusion dryer. Samples are hermetically sealed in a sealing unit (SU), before they are transferred from the glovebox via a pass-through transfer chamber (TC) to the DSC (not shown).

from poly(methyl methacrylate) with an inner diameter of 8.9 cm and an inner tube made of stainless steel wire screen about 2.5 cm in diameter. The annular space between the inner and the outer tube is filled with silica gel drying pearls that are too big to penetrate the wire screen (Silica Gel Orange, Roth, diameter 2−5 mm, specific surface area ∼750 m^2 g^{-1}, water absorbance ∼42 wt % at 80% RH). The aerosol stream is directed through the inner wire-screen tube. While passing through the drying section, water evaporates from the aerosol droplets and diffuses through the wire screen to the annular space where it is absorbed by the silica gel. The dried aerosol then passes the first of two sensors (S1) of a hygrometer (RH; Ahlborn Almeo 2590), which determines the relative humidity of the gas phase of the aerosol. Thereafter, the aerosol particles are collected using a homemade impactor (IM) by accelerating the aerosol stream through a conical glass nozzle (orifice diameter: 1 mm) and directing it onto an impaction plate. In our setup, the impaction plate consists of the bottom piece of a DSC aluminum pan (TA Instruments, hermetic aluminum pan 900793-901), which can be used directly for the subsequent DSC measurements, thus avoiding further sample treatment. Those aerosol particles that pass the impactor without being collected are captured in a HEPA (high efficiency particulate airfilter) filter (F) downstream of the impactor. The filtered gas is directed through a flow meter (FM; Yokogawa Rotameter, model RGC2) for determining the gas volume flow rate through the entire setup. All components are connected either by stainless steel Swagelock fittings and tubing or by plastic tubing. The components RH, IM, F, and FM are placed inside a dry glovebox (GB) about 310 L in volume (dimensions W × D × H: 95 × 50 × 65 cm). During the experiments the relative humidity inside the glovebox is continuously measured with a second sensor (S2) of the hygrometer. Subsequent to sample collection, the aluminum pan is hermetically sealed using a TA Instruments sample encapsulation crimper press (sealing unit, SU) inside the glovebox. Thereafter, the sample pan can be handled in laboratory air for transferring it into the differential scanning calorimeter for further analysis, without running the risk of sample contamination by air.

3.3. Setup Optimization and Test Measurements. To evaluate the working principle and the effectiveness of the MARBLES method, we performed experiments with four reference substances. After numerous tests it proved most practicable to work with a solute mass fraction of $w = 0.02$ for the aqueous solutions feeding the atomizer and an impactor nozzle orifice diameter of 1 mm.

The aerosol drying efficiency depends on the residence time of a particular aerosol particle in the drying section and, therefore, on both the total length of the drying section and the aerosol flow rate. Because the volume flow rate is fixed at ∼1900 sccm due to the operation requirements of the aerosol generator, optimization was achieved by varying the length of the drying section. The relative humidity (RH) of the aerosol gas phase was measured after the drying section and was used as one indicator for a completed aerosol drying process. When a short drying section consisting of a single diffusion dryer tube only is used, the outflow revealed measurable RH values, indicating insufficient drying. However, with a drying section consisting of three diffusion dryer tubes, the monitored RH was always 0% ± 0.1% at a flow rate of ∼1900 sccm. This length-to-flow-rate ratio corresponds to a residence time of an aerosol particle in the drying section of about 37 s. An additional increase of the drying section length did not lead to higher values of T_g in the collected and analyzed samples, which indirectly confirms that the chosen length is sufficient to result in the lowest possible water content, see detailed discussion below.

For the DSC analysis the aluminum pan with the collected aerosol sample was removed from the impactor, sealed hermetically, and then transferred to the DSC. To avoid water uptake by the collected sample during the sealing of the DSC pans with the crimper press, this sealing was done inside a dry glovebox in which the RH was always held below 1%. The effect of water uptake from ambient humidity during sealing on the measured T_g is demonstrated with T_g data of trehalose obtained from the DSC measurements for five different sample preparation cases (Table 1): Sealing the sample inside the dry glovebox where no significant water uptake may either occur immediately (0 s) or occur after waiting for 60 s; immediately sealing the sample in ambient air (0 s) or sealing the sample after exposure to ambient air for 30 s and for 60 s. The glass transition temperature T_g decreases strongly with increasing waiting time before sealing in ambient air and, thus, with increasing exposure time of the sample to the ambient atmosphere. Even if the sample is sealed in ambient air without delay (0 s), the sealing itself takes about 3−5 s and the measured T_g is lower by about 7 K than that of a sample that is sealed inside the dry glovebox. Obviously the 3−5 s needed for sealing is sufficient to adulterate the measured T_g value. Sealing the sample inside the glovebox after a 60 s waiting time did not significantly affect the glass transition temperature, proving that no water is taken up by the sample inside the glovebox. Similar results were obtained with 3-MBTCA (Table 1).

Table 1. T_g of Trehalose and 3-MBTCA Samples after Drying and Exposure to Different Humidity Conditions (Dry Glovebox and Ambient Humidity) for Varying Time Periods before Sealing[a]

sealing conditions	time before sealing [s]	T_g [K] (±2 K)
	Trehalose	
dry glovebox	0	369
dry glovebox	60	368
ambient	0	362
ambient	30	348
ambient	60	340
	3-MBTCA	
dry glovebox	0	305
ambient	0	303
ambient	15	290
ambient	30	284
ambient	45	281

[a] Because ambient humidity varies, all experiments with one substance were done on the same day. A “time before sealing” of 0 s indicates immediate sealing, but we note that the sealing itself takes a few seconds.

For validating the drying effectiveness of the MARBLES method we determined the glass transition temperatures of glucose, sucrose, trehalose, and citric acid. The saccharides were chosen because they are well-studied glass-forming substances, and citric acid was used because it is structurally similar to 3-MBTCA and, thus, it may act as a surrogate in test experiments. In Table 2 we show the T_g values of samples vitrified with the MARBLES setup. All substances were collected under dry conditions for 20 min (resulting in a total mass of up to 5 mg)

Table 2. Glass Transition Temperatures of Reference Compounds Determined with MARBLES and Corresponding Literature Values

substance	T_g [K]	Vitrification procedure and literature references	DSC heating rate [K min^{-1}]
sucrose	331	MARBLES	10
	319	freeze-drying[63]	10
	335	freeze-drying[64]	5
glucose	297	MARBLES	10
	295	melting and cooling[63]	10
citric acid	286	MARBLES	10
	284	melting and cooling[65]	10
	283	melting and cooling[66]	10
trehalose	369	MARBLES	10
	368	freeze-drying[63]	10
	365	freeze-drying[67]	1, 10, and 20
	373	melting and cooling[64]	5
	385	heating of dihydrate at reduced pressure[67]	1, 10, and 20
	388	freeze-drying[68]	10
	388	heating of dihydrate at ambient and reduced pressure[69]	10

and then analyzed by DSC. Also shown for comparison are T_g values of the same substances in which vitrification was achieved by established alternative methods. Given the variability of T_g values reported in the literature, our results agree well with the literature values, providing further support for the applicability of our method for determining T_g of water-soluble organics.

A typical DSC measurement of a heat unstable substance is shown in Figure 3. In this experiment a sucrose sample that had been transferred into the glassy state by the MARBLES method was cooled from 293 to 263 K (blue), heated from 263 to 463 K (green), cooled again to 263 K (magenta), and finally heated to 463 K (red). In the first heating cycle, the transition from a glass to a supercooled liquid occurred as a step in the heat flow signal (1) at 331 K. On further heating, the supercooled liquid first crystallized (2) and then melted (3). In the second cooling and heating cycle again a glass transition was detected (4a and 4b), but now at a lower temperature than in the first heating cycle (309 K). We conclude from this observation that the sucrose underwent chemical changes during the first melting, and that the T_g determined in the second heating cycle has to be assigned to another compound or a compound mixture. In contrast, the glass transition temperature obtained from the sample vitrified at room temperature by the MARBLES method suggests that the sample indeed consists of pure glassy sucrose and, hence, the measured value may represent the "real" T_g of sucrose. In the results section below we show more examples for this kind of behavior and also provide evidence that it is the thermal treatment leading to chemical changes and, thus, a reduced T_g value, and not the MARBLES method that leads to an "artificially enhanced" T_g value.

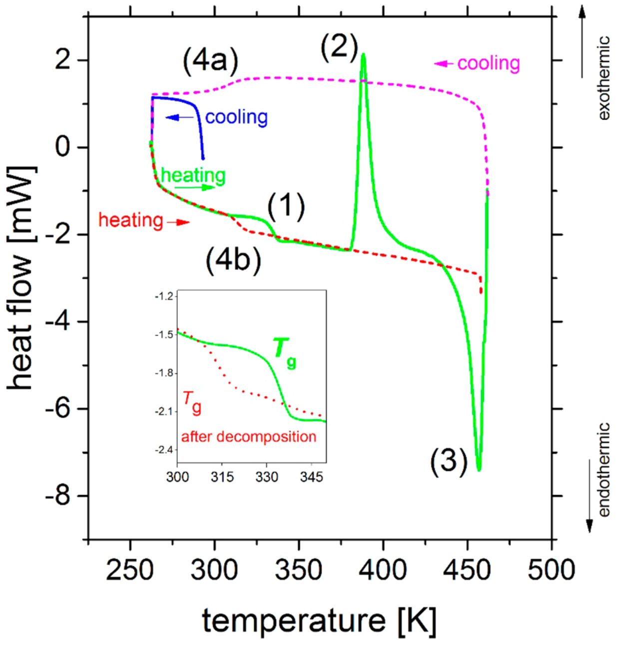

Figure 3. DSC thermogram with two consecutive cooling/heating cycles of the heat-unstable substance sucrose. The first cooling/heating cycle is marked in blue/green, and the second cycle in magenta/red. Numbers indicate the glass transition during the first heating cycle (1), subsequent crystallization (2), and melting/decomposition (3). The glass transition in the second cooling (4a) and heating cycle (4b) is observed at a lower temperature (see inset).

4. THERMAL CHARACTERIZATION OF 3-MBTCA AND MIXTURES THEREOF

4.1. T_g of 3-MBTCA. 3-MBTCA was dissolved in water (w = 0.02) and transferred into the glassy state through the MARBLES process as described above. The collected aerosol sample was then investigated by DSC, Figure 4a. The sample was first cooled from room temperature to 233 K at 10 K min^{-1} and then heated at 10 K min^{-1} to 463 K (green line), before the cooling/heating cycle was repeated (red line). The glass transition (1) was observed at $T_g = 305 \pm 2$ K, which is close to the value predicted from T_m by the Boyer−Beaman relationship $T_{g,pred} \approx 0.7T_m \approx 299$ K.[29] Upon further heating, crystallization (2) of the sample occurred at about 345 K before melting (3) commenced at $T_m = 426$ K, in agreement with a literature value of $T_m = 427$–428 K.[46] In the second cooling cycle only a liquid-to-glass transition was observed and in the second heating cycle a glass transition (4) was detected at about 259 K, i.e., significantly below $T_g = 305$ K of the first cycle. The latter is a clear indication of a chemical change upon melting in the first cycle, and it is in agreement with the fact that no crystallization occurred in the second heating cycle (gray line). In independent experiments we found that upon melting of 3-MBTCA a mixture of the anhydrides **4** and **5** is formed (Scheme 2; see Supporting Informatin for product identification by NMR spectroscopy, mass spectrometry, and IR spectroscopy). Hence, we assign the glass transition temperature $T_g = 259$ K to a mixture of the two anhydrides, residual 3-MBTCA, and water. When a crystalline bulk sample of 3-MBTCA is melted, cooled, and reheated (blue line in Figure 4b), the same low glass transition temperature (4) is observed (compare with the red line, which is reproduced from Figure 4a). This measurement confirms that it is not possible to determine T_g of 3-MBTCA by classical means (heating and cooling) and emphasizes the usefulness of the MARBLES approach taken here. Note that citric acid, a compound that had been used to test the MARBLES approach (Table 2), is structurally similar to 3-MBTCA. Interestingly, citric acid is chemically stable during melting. Chemical changes of citric acid occurred at around 450 K, i.e., well above the melting point

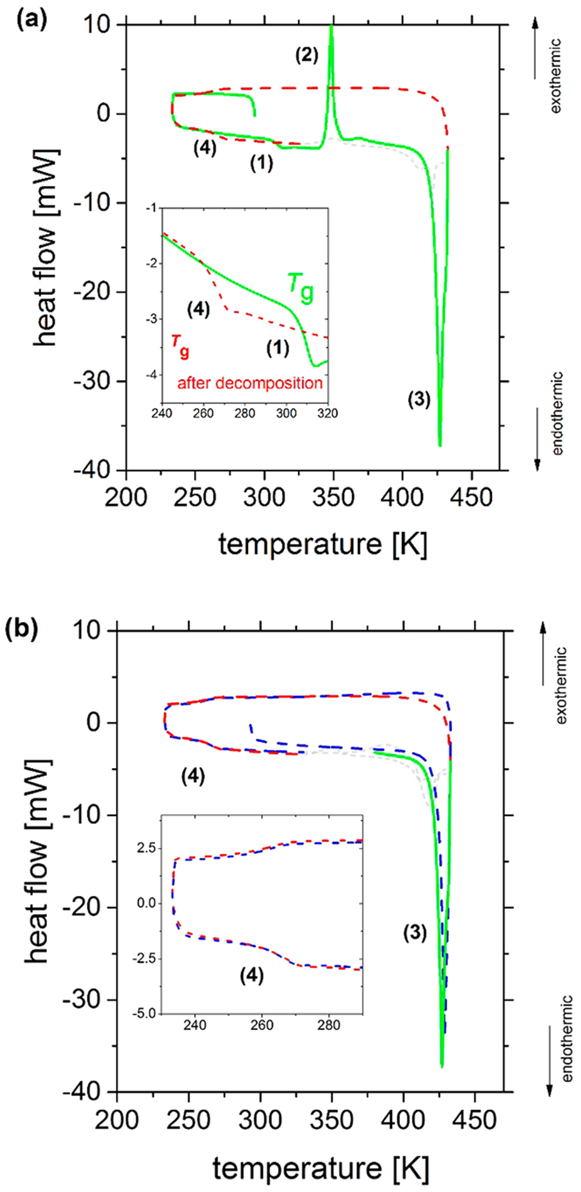

Figure 4. DSC thermograms of 3-MBTCA samples. (a) 3-MBCTA sample collected after the MARBLES process. The first cooling/heating cycle is marked in green, and the second one is marked in red. (b) Comparison of thermograms of a glassy and a crystalline bulk sample of 3-MBCTA. The blue line marks the heating/cooling cycle of the crystalline sample; the red one is reproduced from panel (a). For details, see text.

Scheme 2. Melting of 3-MBTCA Forming the Anhydrides 4 and 5

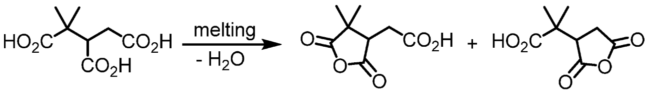

3-MBTCA **4** **5**

of 426 K. IR and ^{1}H NMR spectroscopic data indicate olefin and anhydride formation.

4.2. T_g of Water/3-MBTCA Mixtures. The glass transition temperatures of aqueous solutions of 3-MBTCA are not accessible because of the relatively low water solubility of 3-MBTCA with a solute mass fraction of $w_{sol} \approx 0.24$; see above. Therefore, instead of starting with an aqueous solution, we prepared dry glassy samples of 3-MBTCA by the MARBLES method. We then exposed these bulk samples (2−3 mg) to ambient humidity such that water uptake could occur as described above. The amount of water taken up by these bulk samples was determined by weighing the sample before and after the exposure to humidity. Only samples with water mass fractions of 0.01 and 0.02 (corresponding to exposure times of 1 and 5 min, respectively) could be prepared because longer exposure times did not lead to further water uptake but instead to crystallization of 3-MBTCA in the sample pans. The T_g values for 3-MBTCA mass fractions of $w = 0.99$ and $w = 0.98$ are 289 ± 2 and 272 ± 2 K, respectively. The change of T_g as a function of the water content of a sample can be estimated quite generally with the semiempirical Gordon−Taylor equation:[52]

$$T_g = \frac{w_1 T_{g1} + \frac{1}{k_{GT}} w_2 T_{g2}}{w_1 + \frac{1}{k_{GT}} w_2}$$

Here, T_g is the glass transition temperature of the binary mixture, T_{g1} and T_{g2} are the glass transition temperatures of the two pure compounds, here of water and of solute, w_1 and w_2 are the mass fractions of the two compounds in the mixture, and k_{GT} is the Gordon−Taylor constant. Because T_g of water is very low (T_{g1} = 136 K), even small amounts of water can significantly decrease T_g of the mixture, as found for 3-MBTCA (cf. Table 1). The strong decrease of the water/3-MBTCA mixtures' T_g with only small water content suggests a relatively large Gordon−Taylor constant k_{GT}, and fitting the Gordon−Taylor equation to the available data points results in $k_{GT} \approx 9$. We note, however, that this value can be regarded as a rough estimate only due to the limited available data and the associated uncertainty.

Another important characteristic temperature of aqueous glassy materials is the glass transition of the maximally freeze-concentrated aqueous solution, commonly termed T_g'.[40,53,54] We determined T_g' of 3-MBTCA by studying the phase transitions observed in inverse emulsion samples as described in previous studies.[40] For these measurements an aqueous 3-MBTCA solution ($w = 0.2$) was emulsified by mixing one part of a 7 wt % solution of SPAN60 (Sigma) in a 1:1 mixture of methylcyclopentane/methylcyclohexane (Merck) with one part of the aqueous solution. This mixture was stirred with a homogenizer (IKA Ultra-Turrax T25 basic) for 10 min at 20 000 rpm to yield an inverse emulsion containing aqueous droplets in the micrometer size range. Analysis of such a sample by DSC is shown in Figure 5. Upon cooling at a rate of 10 K min^{-1} (red line) homogeneous ice nucleation occurred at T_h = 229 K, in agreement with a value of 229.5 K predicted by water-activity-based ice nucleation theory[55,56] using the experimentally determined water activity of the aqueous 3-MBTCA solution of a_w = 0.982 at room temperature and a value of $\Delta a_{w,hom}$ = 0.325 for homogeneous ice nucleation in micrometer-sized droplets.[57] Below T_h no further transitions were observed upon cooling to 153 K. Upon heating at 10 K min^{-1} (magenta line) a small exothermic signal was observed above a temperature of 228 K (see also inset), most likely resulting from ice crystal growth that was inhibited during cooling and at lower temperature due to the high viscosity of the freeze-concentrated aqueous 3-MBCTA matrix. At 246 K heating was stopped and tempering of the sample commenced by slowly

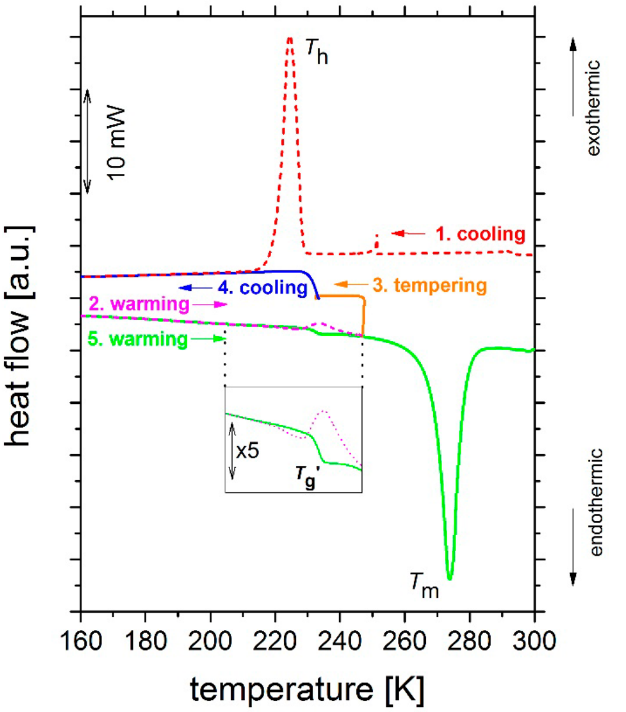

Figure 5. DSC thermogram of an emulsified aqueous solution (w = 0.2) of 3-MBTCA. The red line shows the first cooling, the magenta line shows the heating above T_g', the orange line shows the tempering with a lower cooling rate, and the following cooling and heating are shown by the blue and green lines. T_h indicates homogeneous ice nucleation, T_m the ice melting, and T_g' the glass transition of the maximally freeze concentrated sample. For details, see text.

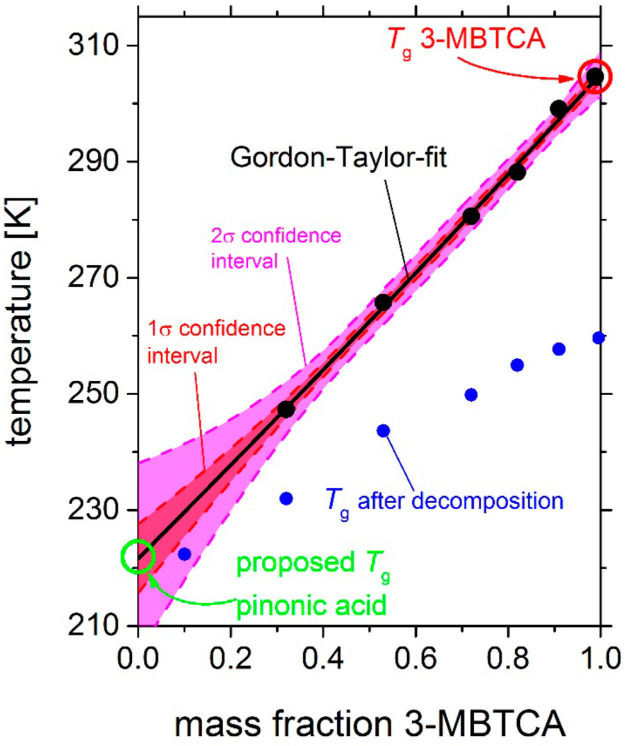

Figure 6. T_g of pinonic acid/3-MBTCA mixtures (black circles) as a function of the 3-MBTCA mass fraction. Also shown are T_g values from the second heating cycle (after chemical changes, blue circles). The red and green circles indicate the measured T_g of pure 3-MBTCA and the proposed T_g of pinonic acid, respectively. The latter results from an extrapolation of the black line obtained from a Gordon–Taylor-fit to the data. The red and pink shadowed areas indicate the 1σ and 2σ confidence intervals of the fit.

cooling the sample to 233 K at 1 K min^{-1} (orange line) before it was cooled further to 153 K at 10 K min^{-1} (blue line). Finally, the sample was reheated to 303 K at 10 K min^{-1} (green line) This time a clear glass transition was observed at 230 K (see also inset), which we assign to the glass transition of the maximally freeze-concentrated solution with a value of T_g' = 230 ± 2 K.

4.3. T_g of Pinonic Acid/3-MBTCA Mixtures. α-Pinene SOA particles consist of different α-pinene oxidation products.[13,14,27] Therefore, we studied T_g of mixtures of the intermediate oxidation product pinonic acid (O:C ratio of 0.3; Figure 1) with the second-generation oxidation product 3-MBTCA (O:C ratio of 0.75). For this purpose we dissolved different mixtures of the two acids with varying mass ratios at an overall mass fraction of about 0.02 in water and then applied the MARBLES procedure. The collected aerosol samples were then analyzed by DSC by first cooling the samples at 10 K min^{-1} to 133 K and then reheating them at 10 K min^{-1} to 433 K. The resulting T_g values are shown as a function of 3-MBTCA dry mass fraction in Figure 6. Clearly, the higher the dry mass fraction of 3-MBTCA the higher is the T_g of the mixture, finally approaching the T_g of pure 3-MBTCA for w_{dry}(3-MBTCA) = 1 in agreement with the Gordon–Taylor equation.[29,52] At lower dry mass fractions w_{dry}(3-MBTCA) < 0.3, i.e., at higher pinonic acid mass fractions, no T_g could be determined owing to crystallization of pinonic acid, in agreement with results of experiments on pure pinonic acid. To describe the T_g of pinonic acid/3-MBTCA mixtures, we fitted the available T_g data to the Gordon–Taylor equation described above, resulting in the black solid line. The fitted line is almost linear ($k_{GT} \approx 1$), thus allowing a relatively stable extrapolation of the T_g curve into the non-glass-forming concentration range at w_{dry}(3-MBTCA) < 0.3. Moreover, the T_g of pinonic acid might be estimated by extrapolating the Gordon–Taylor line to w_{dry}(3-MBTCA) = 0, yielding a T_g of pinonic acid of about 221 K. We note, however, that the Gordon–Taylor approach may result in curved lines for k_{GT} values that are significantly smaller or larger than 1. The pink and red shaded areas indicate, respectively, the 1σ and 2σ confidence intervals of the fitting procedure, representing the very conservative estimates of T_g in the non-glass-forming region.

A T_g of pinonic acid of about 221 K suggests a low or moderate viscosity of supercooled liquid pinonic acid at 293 K, which is too low to prevent crystallization of pinonic acid during the MARBLES procedure, in keeping with experimental observations; see above. Therefore, determining the T_g of pinonic acid requires a modification of MARBLES to allow for particle collection and/or drying at low temperatures.

Also shown in Figure 6 are the T_g values determined in a second cooling and heating cycle. As noted above, 3-MBTCA is converted into the anhydrides **4** and **5** upon melting. Therefore, these T_g values represent the glass transition of mixtures of anhydrides **4** and **5**, water, 3-MBTCA, and pinonic acid. With an increasing amount of pinonic acid, the data approach the T_g proposed for pure pinonic acid. This finding is in agreement with the assumption that pinonic acid is less prone to forming an anhydride.

Finally, in Figure 7 we show the T_g values of several key products of *α*-pinene SOA oxidation as a function of their O:C ratio, a property that is often used to characterize multicomponent SOA particles using aerosol mass spectrometry and also during modeling of SOA oxidation.[13,58,59] The experimental data reveal a clear and almost linear increase of T_g with increasing O:C ratio. This seems to be in contradiction with an analysis in our previous work on the general behavior of T_g in organic molecules: A compilation of data of many very different organic molecules did not show a clear trend of T_g as a function of O:C. Instead, the molar mass dependence of T_g turned out to be much more important.[29] This analysis was a rather general one on a compilation of diverse compounds, however, and an O:C dependence of T_g may hold for specific sets of chemically related compounds only. One such example is the oxidation products of *α*-pinene shown in Figure 7, starting from the pinonaldehyde toward 3-MBTCA. Similar trends of T_g have been suggested for oxidation products identified in SOA derived from specific precursors such as *n*-heptadecane and naphthalene.[60] Hence, we suggest that an O:C dependence of T_g may thus facilitate the prediction of the SOA particles' viscosity and phase state and facilitate modeling their effects on gas-to-particle partitioning and the heterogeneous chemistry of SOA particles.[61,62]

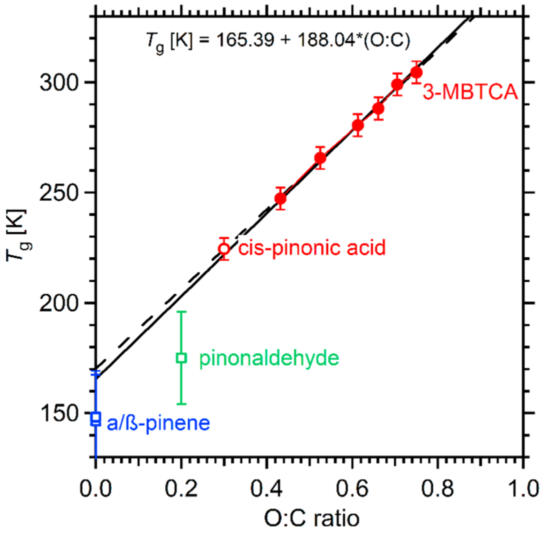

Figure 7. T_g of *α*-pinene oxidation products as a function of the atomic O:C ratio of the compound or compound mixture. The red data points are from Figure 6, the T_g values for *α*-/*β*-pinene and pinonaldehyde were estimated from the Boyer−Beaman relationship (Koop et al.[29]). The dashed black line is a fit to the red data points only, and the solid black line includes all data points with the resulting fit parameters given in the figure.

5. SUMMARY AND CONCLUSION

In this study we have established the MARBLES method based on aerosol diffusion drying as a simple and fast approach to form glassy samples from aqueous solutions. This method is particularly suited for substances that undergo chemical changes upon melting or heating. With MARBLES an aerosol collection time of about 20 min was found to be sufficient for obtaining about 2−5 mg of sample material as is required for a DSC measurement of the glass transition temperature.

We were able to accomplish an efficient synthesis for 3-MBTCA, which is a second-generation oxidation product of *α*-pinene. Several physical and chemical properties of 3-MBTCA were determined such as its solubility in water at room temperature, its melting temperature T_m, its glass transition temperature T_g, and the glass transition temperature of the maximally freeze-concentrated solution T_g'. Furthermore, we have determined the glass-forming properties of 3-MBTCA in mixtures with water and pinonic acid. In particular, the results of pinonic acid/3-MBTCA mixtures suggest a dependence of T_g upon the O:C ratio for a set of compounds that originate from the same precursor along an oxidation pathway. Such a relation may prove helpful for modeling the effects of phase state on the properties and behavior of atmospheric SOA particles.

■ ASSOCIATED CONTENT

Ⓢ Supporting Information

Details of the 3-MBTCA synthesis and of experiments on anhydride formation and associated analytical data, including IR and NMR spectra and TEM images of particles after drying with MARBLES, are presented. This material is available free of charge via the Internet at http://pubs.acs.org.

■ AUTHOR INFORMATION

Corresponding Author

*T. Koop. E-mail: thomas.koop@uni-bielefeld.de.

Author Contributions

The study was conceived by H.P.D., A.G., and T.K., the synthesis was developed and conducted by H.P.D., D.C.S., M.Q., and A.G., the anhydrides were characterized by M.Q., D.C.S., and A.G., the setup was developed and built by H.P.D. and T.K., the experiments were performed by H.P.D., the results were analyzed by H.P.D. and T.K. and discussed by all authors. The paper was written by H.P.D. and T.K. with contributions from all authors. All authors have given approval to the final version of the manuscript.

Notes

The authors declare no competing financial interest.

■ ACKNOWLEDGMENTS

We thank Y. Hertle for taking the TEM images, S. Gunthe for help with the operation of the atomizer and helpful comments on the MARBLES setup, and U. Pöschl for providing the atomizer. H.P.D. acknowledges a Nachwuchsfonds stipend from Bielefeld University.

■ ABBREVIATIONS

CCN	cloud condensation nuclei
DSC	differential scanning calorimetry
IN	ice nuclei
MARBLES	metastable aerosol by low temperature evaporation of solvent
3-MBTCA	3-methylbutane-1,2,3-tricarboxylic acid
O:C ratio	oxygen-to-carbon atom ratio of an organic substance
RH	relative humidity
sccm	standard cubic centimeter
SOA	secondary organic aerosol

■ REFERENCES

(1) Haywood, J.; Boucher, O. Estimates of the Direct and Indirect Radiative Forcing due to Tropospheric Aerosols: A Review. *Rev. Geophys.* **2000**, *38*, 513.

(2) Albrecht, B. A. Aerosols, Cloud Microphysics, and Fractional Cloudiness. *Science* **1989**, *245*, 1227−1230.
(3) Lohmann, U.; Feichter, J. Global Indirect Aerosol Effects: A Review. *Atmos. Chem. Phys.* **2005**, *5*, 715−737.
(4) Koop, T.; Mahowald, N. Atmospheric Science: The Seeds of Ice in Clouds. *Nature* **2013**, *498*, 302−303.
(5) Murray, B. J.; Wilson, T. W.; Dobbie, S.; Cui, Z.; Al-Jumur, S. M. R. K.; Möhler, O.; Schnaiter, M.; Wagner, R.; Benz, S.; Niemand, M.; et al. Heterogeneous Nucleation of Ice Particles on Glassy Aerosols under Cirrus Conditions. *Nat. Geosci.* **2010**, *3*, 233−237.
(6) Andreae, M. O.; Rosenfeld, D. Aerosol−cloud−precipitation Interactions. Part 1. The Nature and Sources of Cloud-Active Aerosols. *Earth-Sci. Rev.* **2008**, *89*, 13−41.
(7) Hoose, C.; Möhler, O. Heterogeneous Ice Nucleation on Atmospheric Aerosols: A Review of Results from Laboratory Experiments. *Atmos. Chem. Phys.* **2012**, *12*, 9817−9854.
(8) Abbatt, J. P. D.; Benz, S.; Cziczo, D. J.; Kanji, Z.; Lohmann, U.; Möhler, O. Solid Ammonium Sulfate Aerosols as Ice Nuclei: A Pathway for Cirrus Cloud Formation. *Science* **2006**, *313*, 1770−1773.
(9) Stocker, T. K.; Qin, D.; Plattner, G.-K.; Tignor, M.; Allen, S. K.; Boschung, J.; Nauels, A.; Xia, Y.; Bex, V.; Midgley, P. M. *IPCC, 2013: Climate Change 2013: The Physical Science Basis*. Contribution of Working Group I to the Fifth Assessment Report of the Intergovernmental Panel on Climate Change; Cambridge University Press: Cambridge, United Kingdom and New York, NY, USA, 2013; p 1535.
(10) Kanakidou, M.; Seinfeld, J. H.; Pandis, S. N.; Barnes, I.; Dentener, F. J.; Facchini, M. C.; Van Dingenen, R.; Ervens, B.; Nenes, a.; Nielsen, C. J.; et al. Organic Aerosol and Global Climate Modelling: A Review. *Atmos. Chem. Phys.* **2005**, *5*, 1053−1123.
(11) Murphy, D. M.; Cziczo, D. J.; Froyd, K. D.; Hudson, P. K.; Matthew, B. M.; Middlebrook, A. M.; Peltier, R. E.; Sullivan, A.; Thomson, D. S.; Weber, R. J. Single-Particle Mass Spectrometry of Tropospheric Aerosol Particles. *J. Geophys. Res.* **2006**, *111*, D23S32.
(12) Zhang, Q.; Jimenez, J. L.; Canagaratna, M. R.; Allan, J. D.; Coe, H.; Ulbrich, I.; Alfarra, M. R.; Takami, A.; Middlebrook, a. M.; Sun, Y. L.; et al. Ubiquity and Dominance of Oxygenated Species in Organic Aerosols in Anthropogenically-Influenced Northern Hemisphere Midlatitudes. *Geophys. Res. Lett.* **2007**, *34*, L13801.
(13) Jimenez, J. L.; Canagaratna, M. R.; Donahue, N. M.; Prevot, A S. H.; Zhang, Q.; Kroll, J. H.; DeCarlo, P. F.; Allan, J. D.; Coe, H.; Ng, N. L.; et al. Evolution of Organic Aerosols in the Atmosphere. *Science* **2009**, *326*, 1525−1529.
(14) Hallquist, M.; Wenger, J. C.; Baltensperger, U.; Rudich, Y.; Simpson, D.; Claeys, M.; Dommen, J.; Donahue, N. M.; George, C.; Goldstein, A. H.; et al. The Formation, Properties and Impact of Secondary Organic Aerosol: Current and Emerging Issues. *Atmos. Chem. Phys.* **2009**, *9*, 5155−5236.
(15) Kroll, J. H.; Seinfeld, J. H. Chemistry of Secondary Organic Aerosol: Formation and Evolution of Low-Volatility Organics in the Atmosphere. *Atmos. Environ.* **2008**, *42*, 3593−3624.
(16) Decesari, S.; Fuzzi, S.; Facchini, M. C.; Mircea, M.; Emblico, L.; Cavalli, F.; Maenhaut, W.; Chi, X.; Schkolnik, G.; Falkovich, A.; et al. Characterization of the Organic Composition of Aerosols from Rondônia, Brazil, during the LBA-SMOCC 2002 Experiment and Its Representation through Model Compounds. *Atmos. Chem. Phys.* **2006**, *6*, 375−402.
(17) Rogge, W. F.; Mazurek, M. A.; Hildemann, L. M.; Cass, G. R.; Simoneit, B. R. T. Quantification of Urban Organic Aerosols at a Molecular Level: Identification, Abundance and Seasonal Variation. *Atmos. Environ. Part A. Gen. Top.* **1993**, *27*, 1309−1330.
(18) Simoneit, B. R. T.; Elias, V. O.; Kobayashi, M.; Kawamura, K.; Rushdi, A. I.; Medeiros, P. M.; Rogge, W. F.; Didyk, B. M. SugarsDominant Water-Soluble Organic Compounds in Soils and Characterization as Tracers in Atmospheric Particulate Matter. *Environ. Sci. Technol.* **2004**, *38*, 5939−5949.
(19) Martin, S. T. Phase Transitions of Aqueous Atmospheric Particles. *Chem. Rev.* **2000**, *100*, 3403−3454.
(20) Marcolli, C.; Luo, B.; Peter, T. Mixing of the Organic Aerosol Fractions: Liquids as the Thermodynamically Stable Phases. *J. Phys. Chem. A* **2004**, *108*, 2216−2224.
(21) Guenther, A.; Hewitt, C. N.; Erickson, D.; Fall, R.; Geron, C.; Graedel, T.; Harley, P.; Klinger, L.; Lerdau, M.; Mckay, W. A.; et al. A Global Model of Natural Volatile Organic Compound Emissions. *J. Geophys. Res.* **1995**, *100*, 8873.
(22) Müller, L.; Reinnig, M.-C.; Naumann, K. H.; Saathoff, H.; Mentel, T. F.; Donahue, N. M.; Hoffmann, T. Formation of 3-Methyl-1,2,3-Butanetricarboxylic Acid via Gas Phase Oxidation of Pinonic Acid − a Mass Spectrometric Study of SOA Aging. *Atmos. Chem. Phys.* **2012**, *12*, 1483−1496.
(23) Zhang, Y. Y.; Müller, L.; Winterhalter, R.; Moortgat, G. K.; Hoffmann, T.; Pöschl, U. Seasonal Cycle and Temperature Dependence of Pinene Oxidation Products, Dicarboxylic Acids and Nitrophenols in Fine and Coarse Air Particulate Matter. *Atmos. Chem. Phys.* **2010**, *10*, 7859−7873.
(24) Yasmeen, F.; Szmigielski, R.; Vermeylen, R.; Gómez-González, Y.; Surratt, J. D.; Chan, A. W. H.; Seinfeld, J. H.; Maenhaut, W.; Claeys, M. Mass Spectrometric Characterization of Isomeric Terpenoic Acids from the Oxidation of A-Pinene, B-Pinene, D-Limonene, and Δ3-Carene in Fine Forest Aerosol. *J. Mass Spectrom.* **2011**, *46*, 425−442.
(25) Szmigielski, R.; Surratt, J. D.; Gómez-González, Y.; Van der Veken, P.; Kourtchev, I.; Vermeylen, R.; Blockhuys, F.; Jaoui, M.; Kleindienst, T. E.; Lewandowski, M.; et al. 3-Methyl-1,2,3-Butanetricarboxylic Acid: An Atmospheric Tracer for Terpene Secondary Organic Aerosol. *Geophys. Res. Lett.* **2007**, *34*, L24811.
(26) Eddingsaas, N. C.; Loza, C. L.; Yee, L. D.; Chan, M.; Schilling, K. A.; Chhabra, P. S.; Seinfeld, J. H.; Wennberg, P. O. A-Pinene Photooxidation under Controlled Chemical Conditions − Part 2: SOA Yield and Composition in Low- and High-NOx Environments. *Atmos. Chem. Phys.* **2012**, *12*, 7413−7427.
(27) Donahue, N. M.; Henry, K. M.; Mentel, T. F.; Kiendler-Scharr, A.; Spindler, C.; Bohn, B.; Brauers, T.; Dorn, H. P.; Fuchs, H.; Tillmann, R.; et al. Aging of Biogenic Secondary Organic Aerosol via Gas-Phase OH Radical Reactions. *Proc. Natl. Acad. Sci. U. S. A.* **2012**, *109*, 13503−13508.
(28) Virtanen, A.; Joutsensaari, J.; Koop, T.; Kannosto, J.; Yli-Pirilä, P.; Leskinen, J.; Mäkelä, J. M.; Holopainen, J. K.; Pöschl, U.; Kulmala, M.; et al. An Amorphous Solid State of Biogenic Secondary Organic Aerosol Particles. *Nature* **2010**, *467*, 824−827.
(29) Koop, T.; Bookhold, J.; Shiraiwa, M.; Pöschl, U. Glass Transition and Phase State of Organic Compounds: Dependency on Molecular Properties and Implications for Secondary Organic Aerosols in the Atmosphere. *Phys. Chem. Chem. Phys.* **2011**, *13*, 19238−19255.
(30) Zelenyuk, A.; Imre, D.; Beránek, J.; Abramson, E.; Wilson, J.; Shrivastava, M. Synergy between Secondary Organic Aerosols and Long-Range Transport of Polycyclic Aromatic Hydrocarbons. *Environ. Sci. Technol.* **2012**, *46*, 12459−12466.
(31) Perraud, V.; Bruns, E. A.; Ezell, M. J.; Johnson, S. N.; Yu, Y.; Alexander, M. L.; Zelenyuk, A.; Imre, D.; Chang, W. L.; Dabdub, D.; et al. Nonequilibrium Atmospheric Secondary Organic Aerosol Formation and Growth. *Proc. Natl. Acad. Sci. U. S. A.* **2012**, *109*, 2836−2841.
(32) Shiraiwa, M.; Seinfeld, J. H. Equilibration Timescale of Atmospheric Secondary Organic Aerosol Partitioning. *Geophys. Res. Lett.* **2012**, *39*, L24801.
(33) Vaden, T. D.; Imre, D.; Beránek, J.; Shrivastava, M.; Zelenyuk, A. Evaporation Kinetics and Phase of Laboratory and Ambient Secondary Organic Aerosol. *Proc. Natl. Acad. Sci. U. S. A.* **2011**, *108*, 2190−2195.
(34) Shiraiwa, M.; Ammann, M.; Koop, T.; Pöschl, U. Gas Uptake and Chemical Aging of Semisolid Organic Aerosol Particles. *Proc. Natl. Acad. Sci. U. S. A.* **2011**, *108*, 11003−11008.
(35) Berkemeier, T.; Huisman, A. J.; Ammann, M.; Shiraiwa, M.; Koop, T.; Pöschl, U. Kinetic Regimes and Limiting Cases of Gas Uptake and Heterogeneous Reactions in Atmospheric Aerosols and

Clouds: A General Classification Scheme. *Atmos. Chem. Phys.* **2013**, *13*, 6663−6686.

(36) You, Y.; Renbaum-Wolff, L.; Carreras-Sospedra, M.; Hanna, S. J.; Hiranuma, N.; Kamal, S.; Smith, M. L.; Zhang, X.; Weber, R. J.; Shilling, J. E.; et al. Images Reveal That Atmospheric Particles Can Undergo Liquid-Liquid Phase Separations. *Proc. Natl. Acad. Sci. U. S. A.* **2012**, *109*, 13188−13193.

(37) Kuwata, M.; Martin, S. T. Phase of Atmospheric Secondary Organic Material Affects Its Reactivity. *Proc. Natl. Acad. Sci. U. S. A.* **2012**, *109*, 17354−17359.

(38) Shiraiwa, M.; Pfrang, C.; Koop, T.; Pöschl, U. Kinetic Multi-Layer Model of Gas-Particle Interactions in Aerosols and Clouds (KM-GAP): Linking Condensation, Evaporation and Chemical Reactions of Organics, Oxidants and Water. *Atmos. Chem. Phys.* **2012**, *12*, 2777−2794.

(39) Angell, C. A. Liquid Fragility and the Glass Transition in Water and Aqueous Solutions. *Chem. Rev.* **2002**, *102*, 2627−2650.

(40) Zobrist, B.; Marcolli, C.; Pedernera, D. A.; Koop, T. Do Atmospheric Aerosols Form Glasses? *Atmos. Chem. Phys.* **2008**, *8*, 5221−5244.

(41) Roberts, C. J.; Debenedetti, P. G. Engineering Pharmaceutical Stability with Amorphous Solids. *AIChE J.* **2002**, *48*, 1140−1144.

(42) Zobrist, B.; Soonsin, V.; Luo, B. P.; Krieger, U. K.; Marcolli, C.; Peter, T.; Koop, T. Ultra-Slow Water Diffusion in Aqueous Sucrose Glasses. *Phys. Chem. Chem. Phys.* **2011**, *13*, 3514−3526.

(43) Singh, S. A Review on Spray Drying: Emerging Technology in Food Industry. *Int. J. Appl. Eng. Technol.* **2014**, *4*, 1−8.

(44) Cal, K.; Sollohub, K. Spray Drying Technique. I: Hardware and Process Parameters. *J. Pharm. Sci.* **2010**, *99*, 575−586.

(45) Yamaguchi, M.; Tsukamoto, M.; Hirao, I. The Michael Reaction of Simple Ester Enolates to α,β-Unsaturated Esters. *Chem. Lett.* **1984**, 375−376.

(46) Alder, K.; Söll, H.; Söll, H. Über Die Indirekte Substituierende Addition. *Justus Liebigs Ann. Chem.* **1949**, *565*, 73−99.

(47) Riechers, B.; Wittbracht, F.; Hütten, A.; Koop, T. The Homogeneous Ice Nucleation Rate of Water Droplets Produced in a Microfluidic Device and the Role of Temperature Uncertainty. *Phys. Chem. Chem. Phys.* **2013**, *15*, 5873−5887.

(48) Tong, H.-J.; Reid, J. P.; Bones, D. L.; Luo, B. P.; Krieger, U. K. Measurements of the timescales for the mass transfer of water in glassy aerosol at low relative humidity and ambient temperature. *Atmos. Chem. Phys.* **2011**, *11*, 4739−4754.

(49) Price, H. C.; Murray, B. J.; Mattsson, J.; O'Sullivan, D.; Wilson, T. W.; Baustian, K. J.; Benning, L. G. Quantifying water diffusion in high-viscosity and glassy aqueous solutions using a Raman isotope tracer method. *Atmos. Chem. Phys.* **2014**, *14*, 3817−3830.

(50) Berkemeier, T.; Shiraiwa, M.; Pöschl, U.; Koop, T. Competition between water uptake and ice nucleation by glassy organic aerosol particles. *Atmos. Chem. Phys. Discuss.* **2014**, *14*, 16451−16492.

(51) Liu, B. Y.; Lee, K. W. An Aerosol Generator of High Stability. *Am. Ind. Hyg. Assoc. J.* **1975**, *36*, 861−865.

(52) Gordon, B. M.; Taylor, J. S. Ideal Copolymers and the Second-Order Transition of Synthetic Rubbers. I. Non-Crystalline Copolymers. *J. Appl. Chem.* **1952**, *2*, 493−500.

(53) Roos, Y. H. Glass Transition Temperature and Its Relevance in Food Processing. *Annu. Rev. Food Sci. Technol.* **2010**, *1*, 469−496.

(54) Corti, H. R.; Angell, C. A.; Auffret, T.; Levine, H.; Buera, M. P.; Reid, D. S.; Roos, Y. H.; Slade, L. Empirical and Theoretical Models of Equilibrium and Non-Equilibrium Transition Temperatures of Supplemented Phase Diagrams in Aqueous Systems (IUPAC Technical Report). *Pure Appl. Chem.* **2010**, *82*, 1065−1097.

(55) Koop, T.; Luo, B.; Tsias, A.; Peter, T. Water Activity as the Determinant for Homogeneous Ice Nucleation in Aqueous Solutions. *Nature* **2000**, *406*, 611−614.

(56) Koop, T. Homogeneous Ice Nucleation in Water and Aqueous Solutions. *Z. Phys. Chem.* **2004**, *218*, 1231−1258.

(57) Koop, T.; Zobrist, B. Parameterizations for Ice Nucleation in Biological and Atmospheric Systems. *Phys. Chem. Chem. Phys.* **2009**, *11*, 10839−10850.

(58) Aiken, A. C.; DeCarlo, P. F.; Kroll, J. H.; Worsnop, D. R.; Huffman, J. A.; Docherty, K. S.; Ulbrich, I. M.; Mohr, C.; Kimmel, J. R.; Sueper, D.; et al. O/C and OM/OC Ratios of Primary, Secondary, and Ambient Organic Aerosols with High-Resolution Time-of-Flight Aerosol Mass Spectrometry. *Environ. Sci. Technol.* **2008**, *42*, 4478−4485.

(59) Donahue, N. M.; Kroll, J. H.; Pandis, S. N.; Robinson, A. L. A Two-Dimensional Volatility Basis Set − Part 2: Diagnostics of Organic-Aerosol Evolution. *Atmos. Chem. Phys.* **2012**, *12*, 615−634.

(60) Saukko, E.; Lambe, A. T.; Massoli, P.; Koop, T.; Wright, J. P.; Croasdale, D. R.; Pedernera, D. A.; Onasch, T. B.; Laaksonen, A.; Davidovits, P.; et al. Humidity-Dependent Phase State of SOA Particles from Biogenic and Anthropogenic Precursors. *Atmos. Chem. Phys.* **2012**, *12*, 7517−7529.

(61) Robinson, E. S.; Saleh, R.; Donahue, N. M. Organic Aerosol Mixing Observed by Single-Particle Mass Spectrometry. *J. Phys. Chem. A* **2013**, *117*, 13935−13945.

(62) Zaveri, R. A.; Easter, R. C.; Shilling, J. E.; Seinfeld, J. H. Modeling Kinetic Partitioning of Secondary Organic Aerosol and Size Distribution Dynamics: Representing Effects of Volatility, Phase State, and Particle-Phase Reaction. *Atmos. Chem. Phys.* **2014**, *14*, 5153−5181.

(63) Simperler, A.; Kornherr, A.; Chopra, R.; Bonnet, P. A.; Jones, W.; Motherwell, W. D. S.; Zifferer, G. Glass Transition Temperature of Glucose, Sucrose, and Trehalose: An Experimental and in Silico Study. *J. Phys. Chem. B* **2006**, *110*, 19678−19684.

(64) Roos, Y. Melting and Glass Transitions of Low Molecular Weight Carbohydrates. *Carbohydr. Res.* **1993**, *238*, 39−48.

(65) Lu, Q.; Zografi, G. Properties of Citric Acid at the Glass Transition. *J. Pharm. Sci.* **1997**, *86*, 1374−1378.

(66) Timko, R. J.; Lordi, N. G. Thermal Characterization of Citric Acid Solid Dispersions with Benzoic Acid and Phenobarbital. *J. Pharm. Sci.* **1979**, *68*, 601−605.

(67) Crowe, L. M.; Reid, D. S.; Crowe, J. H. Is Trehalose Special for Preserving Dry Biomaterials? *Biophys. J.* **1996**, *71*, 2087−2093.

(68) Miller, D.; Pablo, J. de; Corti, H. Thermophysical Properties of Trehalose and Its Concentrated Aqueous Solutions. *Pharm. Res.* **1997**, *14*, 578−590.

(69) Ding, S.-P.; Fan, J.; Green, J. L.; Lu, Q.; Sanchez, E.; Angell, C. A. Vitrification of Trehalose by Water Loss from Its Crystalline Dihydrate. *J. Therm. Anal.* **1996**, *47*, 1391−1405.